



AIAA 2003-0973

Integrated Transition Prediction:
A Case Study in Supersonic Laminar Flow Control

M. Choudhari, C.-L. Chang, C.L. Streett and P. Balakumar
NASA Langley Research Center
Hampton, VA

41st Aerospace Sciences Meeting & Exhibit
January 6–9, 2003
Reno, Nevada

For permission to copy or to republish, contact the copyright owner named on the first page.
For AIAA-held copyright, write to AIAA Permissions Department,
1801 Alexander Bell Drive, Suite 500, Reston, VA, 20191-4344.

INTEGRATED TRANSITION PREDICTION: A CASE STUDY IN SUPERSONIC LAMINAR FLOW CONTROL

Meelan Choudhari[†], Chau-Lyan Chang^{††}, Craig Streett^{†††} and P. Balakumar^{*}
NASA Langley Research Center, Hampton, VA 23681

Abstract

Laminar flow control (LFC) is one of the key enabling technologies for quiet and efficient supersonic aircraft. Recent work at Arizona State University has led to the development of a novel concept for passive LFC on crossflow dominated flow configurations. It employs distributed leading-edge roughness to limit the growth of naturally dominant instabilities that would otherwise lead to an earlier onset of transition. LFC technology development under DARPA's Quiet Supersonic Platform (QSP) and NASA's Supersonic Vehicle Technology (SVT) programs includes both wind-tunnel and flight experiments aimed at further development of roughness based LFC at close to full-scale Reynolds numbers, and design studies for integrating this new concept into the overall vehicle design. Companion theoretical studies at NASA Langley Research Center have the objective of providing both an enhanced physical understanding to facilitate the optimization of roughness based LFC, and a physics based transition prediction capability for this and other LFC configurations. This paper outlines the findings based on a preliminary exploration of the parameter space, in terms of receptivity plus linear and nonlinear development of stationary crossflow instabilities on an infinite-span swept airfoil at a free-stream Mach number of 2.4 and chord Reynolds number of 16.3 million. The findings are used to advocate a holistic approach for transition prediction, which

accounts for all major stages within transition (namely, receptivity, linear growth, nonlinear interactions and secondary instability) in an integrated manner.

1. Introduction

Given the recently renewed quest for long-range supersonic flight, both DARPA and NASA have partnered with industry and universities to help develop the next generation of supersonic vehicles after Concorde. Future efforts under DARPA's Quiet Supersonic Platform (QSP) program^[56] will focus on a long-range strike military vehicle, while NASA's Supersonic Vehicle Technology (SVT) program is geared towards key technologies that would enable the future fleet of supersonic transports to be "indistinguishable from its subsonic counterpart in terms of safety and environmental capabilities."^[25] Common to both programs is the pursuit of aggressive performance goals, to help meet the mission requirements of a military vehicle and to ensure the economic and environmental viability of a civilian transport.

Laminar flow control (LFC) is one of the key technologies being addressed under the above programs. Bushnell^[3] points out the cascading benefits from LFC, namely, drag reduction, reduced weight, increased range, lower sonic boom, and reduced noise levels and emissions. The relevant LFC concepts include both

[†] Aerospace Technologist, Computational Modeling and Simulation Branch, Senior Member AIAA
Email: m.m.choudhari@larc.nasa.gov

^{††} Aerospace Technologist, Computational Modeling and Simulation Branch, Senior Member AIAA

^{†††} Aerospace Technologist, Computational Modeling and Simulation Branch.

^{*} Aerospace Technologist, Flow Physics and Control Branch, Senior Member AIAA

Copyright © 2003 by the American Institute of Aeronautics and Astronautics, Inc. No copyright is asserted in the United States under Title 17, U.S. Code. The U.S. Government has a royalty-free license to exercise all rights under the copyright claimed herein for Governmental Purposes. All other rights are reserved by the copyright owner.

traditional techniques involving either passive control based on tailoring of the inviscid pressure gradient,^[30] active stabilization via surface suction^[1] and/or surface cooling^[7, 44]; and the recently proposed concept of using artificially introduced surface roughness to delay crossflow-induced transition^[47, 50]. The latter technique, proposed by Saric and his coworkers at Arizona State University (ASU), is particularly noteworthy for being the only passive technique that is applicable to crossflow dominated transition and incurs minimal additional penalties associated with control. Another potential concept for LFC involves the use of surface permeability, which has been shown to damp the growth of second mode instabilities at hypersonic speeds.^[21, 35] Conceivably, analogous benefits may accrue in the case of first mode and/or non-stationary crossflow instabilities after suitable tuning of the surface impedance characteristics. Given the merits and limitations of each individual LFC technique, an optimal implementation of supersonic LFC (SLFC) would likely involve a synergistic combination of multiple concepts (i.e. a hybrid approach analogous to subsonic LFC), either on the same aerodynamic surface or on the vehicle as a whole.

As discussed by the National Research Council panel on Breakthrough Technology for Commercial Supersonic Aircraft^[39], stringent requirements for component performance plus economic and environmental challenges for a supersonic aircraft leave little room for inefficiencies in airframe design. Therefore, irrespective of the choice of LFC technique(s), it is necessary to have accurate and reliable prediction tools for the transition process. Although N-factor correlations based only on linear growth characteristics have been shown to be reasonably accurate in a broad range of flows, they offer rather limited scope for further refinement. More significantly, their limitations for transition prediction in crossflow dominated flows have become particularly apparent during recent studies based on low-speed wind tunnel experiments at ASU^[42, 47] and at NASA Langley Research Center^[13, 31, 53].

The studies mentioned above have shown that linear stability alone is unlikely to predict the dominant spectrum of instability modes in swept-wing boundary layers because of the preferential excitation of stationary crossflow modes in a sufficiently benign unsteady disturbance environment^[14]. Furthermore, the extended length of nonlinear interactions during crossflow-dominated transition, together with the prolonged region of laminar breakdown at higher speeds, indicates a strong need for embedding the nonlinear stage into the transition prediction process for supersonic swept-wing flows. For example, in the context of controlled laboratory experiments at low speeds, an N-factor criterion based on the linear amplification of secondary

instabilities has been shown to provide more accurate transition onset predictions than either a linear N-factor or an absolute amplitude criterion based on the primary instability alone^[33].

The ASU concept for roughness based transition control^[47] clearly illustrates the emerging need for advanced transition prediction techniques, initially as a source of supplementary information and eventually towards high-fidelity analysis during aerodynamic design. The ASU concept utilizes controlled leading-edge roughness to introduce subdominant (stationary) crossflow modes that are unlikely to cause transition on their own. However, because of their stronger amplification immediately downstream of the location of excitation, these modes tend to suppress the initial growth of naturally dominant modes and, hence, delay the onset of transition. Because this concept is predicated on the process of nonlinear mode competition, which in turn is achieved via artificial receptivity, this new LFC concept inherently relies upon physical mechanisms not reflected in the linear stability based predictions. Finally, in addition to the potential practical benefits derived from this mode of LFC, the ASU concept also provides for a relatively “controlled” transition process; this makes it easier to apply an advanced transition prediction approach that mimics the actual transition process in terms of most or all of its major stages. In other words, roughness based control also provides a useful test bed, intermediate in complexity, against which to calibrate the holistic or integrated transition prediction approach.

The individual ingredients of such an approach have previously been developed and tested in the context of swept airfoil configurations, both within our group^[5, 8-10, 13, 15, 28, 32-33, 40, 46, 51-52] and elsewhere.^[17-18, 23-24, 26-27, 38, 41]

Integration of these ingredients in the context of a purely natural disturbance environment was attempted during the analysis of measured data from the NASA/Boeing Hybrid Laminar Flow Control (HLFC) experiment.^[13, 31, 53] Disturbance measurements downstream of the leading edge were used in conjunction with computations to estimate the initial spectrum at an upstream location, which in turn served as the starting point for further investigation^[13] based on nonlinear parabolized stability equations^[2, 24] (PSE) and secondary instability calculations.

Much of the previous work, especially pertaining to roughness-based control, has been carried out for low-speed configurations and relatively small chord Reynolds numbers ($Re_c = O(2-3 \times 10^6)$). The physics of stationary crossflow modes is not particularly sensitive to Mach number effects, at least through the low supersonic range. However, higher Reynolds numbers coupled with supersonic flow speeds pose inherent hurdles to any form

of LFC. The challenges at higher Reynolds numbers include both technical aspects (related to highly unstable boundary layers) and those related to practical implementation (because of magnified sensitivity to various factors that cannot be easily controlled in a realistic flow environment, particularly when the form of control is purely passive) [Bushnell, private communication, 2001]).

Considerable work is currently in progress under the QSP and SVT programs to address and overcome the high-Reynolds-number challenges in the context of roughness based LFC, including wind tunnel experiments at intermediate and full-scale Reynolds numbers. Related work at NASA Langley Research Center involves the development and application of higher fidelity transition prediction tools. Major aspects of the tool development are addressed in a companion paper^[8]. The objective behind the present work is to examine design and optimization of roughness-based LFC within the framework of the holistic approach to transition. A comprehensive theoretical study to meet this goal is currently underway. The present paper outlines the findings from the initial phase of this study, which was aimed at assessing the capability of the advanced design tools at higher Reynolds numbers; identifying specific areas for validation; and formulating a strategy for a systematic parametric study in follow-on work.

To help meet these objectives, we examine the highest Reynolds-number condition ($Re_c = 16.3$ million based on mid-span, streamwise chord) from the ASU Mach 2.4 wind tunnel experiments documented by Saric and Reed^[50]. The feasibility of roughness based transition delay has already been demonstrated for this configuration. The theoretical findings reported herein are intended to provide *a posteriori* insights into the details of the underlying flow phenomena. Linear and nonlinear development of crossflow instabilities in the boundary layer over this configuration is examined in Section 2 below. These results establish the potential significance of the initial amplitudes of both the control input and the naturally occurring crossflow instabilities towards their subsequent nonlinear development and, hence, the onset of transition. Accordingly, the generation of stationary crossflow instabilities in a supersonic boundary layer by short-scale non-uniformities in surface geometry is studied in Section 3. An initial attempt to characterize the surface roughness over a representative aerodynamic surface is outlined in Section 4. Concluding remarks and an outline of future work, is presented in Section 5.

All of the stability results reported in this paper have been obtained using the Langley Stability and Transition Analysis Code (LASTRAC). LASTRAC is a third-

generation PSE code developed by Chang and coworkers,^[5, 6, 8] designed to improve on its previous versions via better algorithms and modern software engineering practices. Currently, it includes modules to solve the quasi-parallel stability equations and linear and nonlinear versions of PSE for compressible shear flows that are invariant along one spatial direction (e.g., infinite-span airfoil flows and axisymmetric bodies at zero angle of attack). However, we envision that LASTRAC will eventually include a suite of codes allowing transition prediction at hierarchical levels of prediction accuracy, required input data and/or computational resources (Fig. 1).

2. Linear and Nonlinear Development of Crossflow Modes in a Supersonic Swept-Wing Boundary Layer

The LFC experiments reported in ref. [50] were conducted in the M 2.4 ASU 0.2-m Supersonic Tunnel. The swept-wing model had a leading-edge sweep of 73 degrees, 0.3 meter streamwise chord at the mid-span location and a symmetric cross section with thickness-to-chord ratio of 4%. The cross section of this airfoil was designed to be conducive to the passive, roughness-based control strategy. Specifically, it features a small enough leading-edge radius (to ensure laminar flow along the attachment line) and a favorable pressure gradient extending through at least 80% of the chord (to promote crossflow modes over first mode, i.e. streamwise instabilities). Three different Reynolds numbers were considered in the experiments, ranging from $Re_c = 8.7$ million to 16.3 million. Because the present work focuses on higher Reynolds number effects, the $Re = 16.3$ million configuration is used for the results presented herein.

For the current study, the mean flow was modeled as (locally) invariant along the span. In reality, of course, the presence of tunnel walls may have caused the surface pressure distribution to deviate from the conical or infinite-span approximation (which would be more relevant to external flight conditions). Based on the surface pressure prediction in Fig. 2 of ref. [50] and assuming adiabatic thermal conditions at the model surface, the mean boundary-layer flow was computed using the BLSTA code^[55] and was subsequently used during the linear and nonlinear stability calculations described in this section.

2.1 Linear stability characteristics

2.1.1 Stationary crossflow modes and the effects of nonparallel mean flow and surface curvature

Because the stability predictions used to design the control scheme for the ASU experiments were based on quasi-parallel stability theory without the effects of surface curvature, it is useful to begin with an assessment of mean-flow nonparallelism and surface curvature on the predicted linear growth characteristics of the stationary crossflow modes. Figures 2(a) and 2(b) display the N-factor predictions (i.e., integrated amplification ratios relative to an approximate neutral location) based on linear PSE including the effects of surface curvature (NPWC) for spanwise wavelengths ranging from less than 1 mm to 12 mm. Figure 3 shows a comparison of the associated growth rates with those based on the quasi-parallel approximation, both with and without surface curvature effects (QPWC and QPNC, respectively), and nonparallel predictions without curvature (NPNC) for selected wavelengths of the disturbance modes.

Figure 2(a) illustrates the large magnitudes of N factors involved (reaching $N=9$ by 30% chord and $N=23$ by 85% chord) and the relatively broad range of wavelengths (2 mm to 6 mm) corresponding to high amplification ratios over a dominant portion of the chord. Both of these features are symptomatic of high Reynolds-number flows and are indicative of the challenges involved in successfully implementing LFC in such flows. The results from Fig. 2(b) also suggest that the composition of the surface roughness, especially narrow peaks in its spatial spectrum, are likely to play an important role in determining the identity of the naturally dominant mode(s), i.e., the targets of control action during LFC.

As expected, effects of both nonparallel mean flow and the surface curvature are most significant near the leading edge. Because this region plays a crucial role in the roughness based LFC technique, it seems desirable to include both of these effects during the preliminary design process, even if purely linear tools are used for this purpose. Overall, the destabilizing effects of nonparallel mean flow are partially nullified by the stabilizing influence of convex curvature. This cancellation brings the growth rate predictions based on QPNC in close alignment with the nonparallel growth rates including the effects of curvature (NPWC), except at the larger wavelengths for which nonparallel effects are relatively more significant. These findings are consistent with a number of earlier studies in the context of low-speed flows.

The LASTRAC predictions for linear disturbance evolution in a variety of canonical flow configurations have been cross-validated against a high-order DNS code, DNSUTA, developed at the University of Texas at Arlington^[29]. A detailed comparison based on this study will be reported in a separate forthcoming paper^[28]. Herein, we simply indicate the comparison pertaining to linear amplification of a stationary crossflow mode in a supersonic, swept-wing boundary layer.

The model geometry used for this comparison is based on a moderate-Re, subsonic-leading-edge configuration designed for hybrid laminar flow control. It involves a leading-edge sweep of 80.8 degrees and mimics a specific cross-section of the F16-XL glove used during a previous flight experiment involving suction based LFC.^[1] It also mimics the zero-suction delta-wing configuration used for related precursor experiments in the Supersonic Low Disturbance Tunnel at NASA Langley Research Center.^[4] Earlier simulations pertaining to this case were presented in Ref. [40]. Compared with the higher-Re ASU configuration examined in the present paper, this other configuration allows a well-resolved simulation without requiring an excessively large number of computational grid points. In the DNS computation, the stationary vortex mode was excited by a spanwise-periodic array of roughness elements analogous to those used for passive LFC applications. The N-factor comparison in Figure 4 clearly demonstrates satisfactory agreement between LASTRAC predictions and the DNS computations (after the DNS results merged with the eigensolution at $x > 0.14$). Because of the relatively earlier asymptote of the temperature perturbations to an eigenmode behavior, N factors based on the peak temperature perturbation have been used for the comparison shown in Fig. 4.

2.1.2 Non-stationary crossflow modes

Linear growth predictions for non-stationary (i.e., traveling) crossflow modes are shown in Figs. 5(a) and 5(b) for spanwise disturbance wavelengths of $\lambda_z = 3$ mm and $\lambda_z = 1.5$ mm, respectively. The disturbance wavelength of $\lambda_z = 3$ mm corresponds to the most unstable stationary crossflow mode from Fig. 2(a). The wavelength of 1.5 mm is appropriate for the stationary control input used for roughness-based LFC.

Consistent with previous experience based on a large body of swept-wing flow configurations, the growth factors for traveling modes are significantly larger than those for the stationary modes. Similar to their stationary counterparts, traveling modes at $\lambda_z = 3$ mm continue to amplify throughout the chordwise region shown in Fig. 5(a), whereas the traveling modes at the shorter spanwise wavelength (Fig. 5(b)) begin to decay

somewhat upstream of the upper branch neutral location for the stationary modes ($f=0$).

The disparity between the linear growth of traveling and stationary modes is particularly striking in this example because of the already large N-factors for the stationary crossflow modes. The difference between peak N factors for the stationary and non-stationary modes is as large as 20 for $\lambda_z = 3\text{mm}$ and almost 12 for $\lambda_z = 1.5\text{mm}$. Indeed, the peak N factors are more than doubled in the latter case. Thus, again, the issue of whether (or when) and why such enormously large linear growth potential might be suppressed in favor of stationary modes cannot be answered without further knowledge of the unsteady disturbance environment and the associated receptivity mechanisms. In the context of the nonlinear calculations presented later, we attempt to gain additional clues in this regard by considering the evolution of relatively small amplitude traveling modes in the presence of higher amplitude stationary vortices.

2.2 Nonlinear development of stationary modes

As demonstrated in the course of the ASU wind tunnel experiments, linear stability results can provide useful information for preliminary design of roughness based LFC, particularly with respect to location and spacing of the artificial roughness elements. Of course, purely linear tools are insufficient to arrive at an optimal set of parameters for the control scheme. Furthermore, due to the intrinsically nonlinear nature of this control concept, linear theory fails to indicate to what extent laminar flow is achievable for the chosen scheme. Nonlinear modal interactions must be considered for this purpose. To gain some insights into the effects of disturbance nonlinearity in the configurations of interest, we now examine elementary classes of nonlinear interactions between stationary (and, to a lesser degree, non-stationary) crossflow modes in this section. Again, we emphasize that the primary purpose behind these cases is to pave the way to a comprehensive parametric investigation pertaining to higher-Re swept-wing configurations. Consequently, no attempt has been made to model the observed transition locations (either without or with control) during the ASU experiment at this stage.

Purely for convenience, most of the nonlinear calculations described herein have been initiated with linear eigenfunctions (together with a specified amplitude spectrum) at $x/c \approx 0.075$, which is the first location where an unstable eigenmode could be easily found for the longest wavelength mode (12 mm) included in this study.

2.2.1 Single mode development

Previous work on low-speed configurations (the NLF-0415(b) airfoil used in ASU investigations^[42, 47] and the FLOW-9 model employed in the NASA/Boeing HLFC experiment^[13, 31, 53]) indicates that the natural evolution of stationary crossflow instabilities tends to be dominated by the most unstable linear modes. Accordingly, we first consider the nonlinear evolution of a single stationary mode with a spanwise wavelength of 3mm. Chordwise evolution of the fundamental and its first harmonic for various initial amplitudes (measured in terms of the peak perturbation in chordwise velocity relative to the free-stream speed) is shown in Fig. 6(a). For sufficiently large initial amplitudes (cases $A(x_i) = 10^{-4}$ and 10^{-5} in Fig. 6(a)), the fundamental amplitude reaches a peak at amplitudes in excess of 12 percent (on this scale), then decreases somewhat before continuing to increase further and achieving another peak. The chordwise location of the local minimum and the subsequent maximum in the fundamental evolution correspond approximately to a maximum and minimum, respectively, in the accompanying evolution of the first harmonic. This behavior suggests a cyclic energy exchange between the two modes. When the initial amplitudes are low (cases $A(x_i) = 10^{-6}$ and 10^{-7} in Fig. 6(a)), the fundamental evolution does not display any local minimum, at least within the range of computations plotted in Fig. 6(a). The fundamental amplitude continues to increase in a monotonic fashion until reaching disturbance amplitudes of about 15 percent. Overall, the amplitude evolution curves indicate a relatively uniform upstream shift (at least through the initial rise of the primary amplitudes) as the initial vortex amplitude is increased across the range considered in Fig. 6(a).

The above features of nonlinear development are at least partially analogous to those observed in previous literature in the context of lower-Re configurations. The major difference appears to be in the relative rates at which the peak amplitudes are achieved. For the lowest initial amplitude, for example, the fundamental amplitude ascends from just 1% to nearly 15% across only 12 percent of the overall chord. In less unstable configurations such as the low-speed ASU configuration based on NLF-0415(b) airfoil section,^[23, 33, 47] the primary vortex amplitude was found to vary at a relatively slower rate (indicating an extended quasi-equilibrium state). Consequently, a small but finite lag was noted between the onset of a high-frequency secondary instability^[33] and the measured transition location^[42, 47]. Given the seemingly faster rise in fundamental amplitudes in the present configuration, it will be interesting to see whether this lag is considerably reduced, causing transition to occur rather immediately after the secondary instability sets in.

The potentially shorter region of secondary instability on the present class of high-Re configurations would have an interesting implication for transition prediction within the holistic framework. Secondary instability is known to exhibit a threshold behavior with respect to primary disturbance amplitudes. If it can be established that the primary amplitudes along the rapidly rising portion of the primary amplitude curve are large enough for the secondary instability to set in, then the complicated and time-consuming task of secondary instability predictions could be abandoned in favor of a simpler transition criterion based on the amplitude of the primary disturbance alone.

Indeed, the normalized velocity contours plotted in Fig. 6(b) indicate a strong possibility that the onset of secondary instability will occur well before the peak amplitudes in Fig. 6(a) have been reached. The contours shown in Fig. 6(b) correspond to a chordwise location of $x/c \approx 0.62$ for the case of $A(x_i) = 10^{-7}$ in Fig. 6(a). During prior work,^[10] similar overturning of the velocity contours and the resulting regions of high shear away from the wall have been correlated with the onset of high-frequency secondary instabilities. Of course, additional parameter studies particularly for realistic initial amplitude spectra are necessary to establish the generality of the strongly non-equilibrium nature of disturbance evolution noted above.

We also note that after the fundamental amplitude in the nonlinear PSE calculations became sufficiently large (nearly 15% in Fig. 6(a)), the shape functions for the associated pressure disturbance developed significant two-point oscillations that are characteristic of the odd-even decoupling caused by the non-staggered discretization scheme employed in LASTRAC. The computations could certainly be continued well downstream of the onset of these spurious oscillations (through what appeared to be a post-saturation stage following the second peak in case of the higher initial amplitudes in Fig. (6a)); furthermore, the velocity and temperature disturbances remained smooth even after the oscillations in the pressure disturbance became significantly large. Quite possibly, the spurious oscillations can be eliminated via judicious choice of grid clustering in the wall-normal direction and may not have a serious impact overall, especially if the disturbance amplitudes prior to their onset are already large enough to initiate the onset of transition. However, pending further investigation into the effect of these oscillations on the overall accuracy of the solution, we have typically omitted the questionable regions (always in the vicinity of the peak vortex amplitude) from our results.

We now consider the (isolated) nonlinear development of shorter wavelength, subdominant stationary modes,

which are suitable as the control input for roughness based LFC. For this purpose, the ASU experiments^[50] used a roughness spacing of $\lambda_z = 1.7$ mm because the stationary mode at this wavelength (among others) satisfies the following criteria based on low-speed investigations. Specifically, it has a somewhat earlier onset of linear instability compared with the most unstable mode(s) and a shorter region of linear amplification (which prevents this mode from achieving amplitudes large enough to cause transition on its own). A typical nonlinear evolution for a single mode with $\lambda_z = 1.71$ mm is presented in Fig. 6(c). Due to nonlinear effects, this mode begins to decay much earlier than its theoretical neutral location. Similar behavior is indicated for the 1.5 mm mode (which also satisfies the abovementioned criteria) and even at $\lambda_z = 2$ mm (which has a relatively large linear N-factor). Because of the closer harmonic relationship of the 1.5 mm mode to the dominant 3mm mode, the 1.5 mm mode is used in the following subsection to illustrate its control action on the dominant mode.

The effect of varying the initial amplitude of the 1.71 mm mode on its subsequent development is shown in Fig. 6(d), which includes a few computations that were initiated just downstream of the attachment line. The results indicate that the earlier, nonlinear decay of this mode persists through a wide range of initial amplitudes. The peak amplitude of this mode never exceeds 10%, but a double peak appears for sufficiently large initial amplitudes. These characteristics confirm the suitability of this mode for roughness-based LFC within the upstream portions of the chord. Also observe that the location and streamwise extent of the peak amplitude region (responsible for maximum control action) is substantially influenced by the initial amplitude parameter. Because of the relatively short region over which the subdominant mode appears to sustain its peak amplitudes, it is possible that a multi-stage control (based on additional control input via another mode that is active over the mid-chord region) might be useful for high-Re applications of roughness-based LFC.

2.2.2 Two-mode interaction

To simulate the effects of roughness based LFC in the simplest possible framework, we now consider the effect of nonlinear interaction between the subdominant 1.5 mm mode and the most unstable 3 mm mode. Figure 7(a) displays the effect of the magnitude of control input (i.e., initial amplitude of the 1.5 mm mode) on the subsequent evolution of the target mode with $\lambda_z = 3$ mm. The initial amplitude of the naturally dominant target mode was held fixed at 10^{-5} in each of these cases. Obviously, within the range of parameters considered in Fig. 7(a), successive increases in control input produce the beneficial effect of delayed growth of the target mode.

The suppression of the dominant mode appears to correlate qualitatively with the behavior of the mean flow correction associated with the control mode. Specifically, suppression of target mode growth rates begins only after the control mode has achieved significant amplitudes, but continues past the peak of the 1.5 mm mode. The evolution of the mean-flow correction (u_{00} mode in Fig. 6(c)) indicates a similar lag with respect to the modal amplitudes at $\lambda_z = 1.71$ mm.

For all of the cases in Fig. 7(a), there is a relatively disturbance free zone following the decay of the control input and prior to the inevitable rise of the target 3 mm mode. Except for an effectively reduced initial amplitude, this rise is analogous to the single mode development in Fig. 6(a). Accordingly, the speculative comments pertaining to transition prediction in the single mode case are also relevant to the controlled case. Thus, if the peak amplitudes of the 1.5 mm mode do not lead to premature transition (which is likely because of the narrow region of peak amplitudes for this mode), then a primary-amplitude criterion of the type discussed in section 2.2.1 may be relevant to the controlled case as well. Specifically, the primary-amplitude criterion would enable a relatively straightforward assessment of each increase in the initial control input in terms of resulting shift in the transition onset location, via accompanying horizontal shifts in the primary amplitude curve. For example, increasing the control input from case (d) to case (a) in Fig. 7(a) might produce a transition delay of approximately 20 percent of the model chord.

Analogous results in Fig. 7(b) indicate that the role of variations in the initial amplitude of the target 3 mm mode is analogous but opposite to that of variations in the control input. This indicates the significance of the relative initial amplitudes of the two modes involved in the interaction. Also observe that the streamwise extent of the low-disturbance region following the peak of the 1.5 mm mode narrows progressively at larger initial amplitudes of the target mode.

A preliminary calculation to assess the role of control input in the form of a slower growing, larger wavelength mode (6 mm in this case) was also carried out. Within an intermediate range of locations, a phase locked interaction between the control input and its linearly unstable harmonic actually led to an increased growth rate of the target mode ($\lambda_z = 3$ mm) above its linear value. However, after reaching sufficiently large amplitudes farther downstream, the subharmonic mode did contain the 3 mm mode to lower amplitudes than it might have achieved without any control input. Of course, further analysis is necessary to ensure that the combined flowfield does not exhibit an earlier onset of secondary instabilities than might be expected on the basis of modal evolution alone.

The possibility of subharmonic control has been noted in prior calculations of roughness-based LFC^[27]. However, the combined effect of control input involving both shorter and longer wavelength subdominant modes needs to be investigated. Because the two classes of modes may be active in different regions of the chord, a combined approach might conceivably be more effective than using either mode alone. Any excess growth of the target mode in localized regions might potentially be avoided using a suitable larger wavelength mode (that does not bear a close harmonic relationship to the most unstable target modes) and/or through a suitable phase lag between the control and target modes as presented below.

2.2.3 Two-mode interaction: effect of relative phase

Sample calculations were also made to investigate the effects of the relative initial phase on the downstream evolution of the two-mode interaction. Modal evolution for three selected values of the phase difference parameter (measured as the phase of the peak chordwise velocity perturbation for the target mode at the initial location, relative to that of the control input) is shown in Fig. 8. These results suggest that intermodal phase differences can potentially influence the ensuing evolution of the modes participating in the nonlinear interaction. An examination of the corresponding growth rates (not shown here) indicates that the maximum suppression of the 3mm mode in the 90 degree case (relative to the other two cases) occurs near the 20 percent chord location, i.e., close to the peak amplitude of the 1.5 mm mode. Note that the value of 90 degrees has no particular significance, as the optimal phase difference is likely to vary with the initial location.

Effects of relative phase between an energetic fundamental and its lower amplitude subharmonic are well documented for non-stationary instabilities in free-shear flows^[36] and boundary layers^[49]. Whether a similar mechanism would explain the effects observed in Fig. 8 is unknown. Further calculations are also necessary to confirm this finding and to establish its generality. Indeed, one of our earlier calculations for the low-speed ASU configuration^[47] did not reveal any phase dependency of this type.

If the effects of the relative phase prove to be significant, it could open up an additional avenue (albeit perhaps not a practical one) to influence the nonlinear crossflow evolution. Phase scrambling in a broadband environment also has the potential to render the nonlinear mean state less unstable to high-frequency secondary instabilities for a given level of disturbance energy. Finally, uncertainties associated with modal

phases would indicate the need for a stochastic prediction approach such as that investigated in ref. [46] for triadic and other interactions.

2.2.4 Three mode interactions

The primarily bimodal interactions (not including the universal mean-flow correction) examined in Sections 2.2.2 and 2.2.3 were limited to a fundamental mode of selected wavelength and its first harmonic. Similar interactions between other modes (3 mm and 1.71 mm; 3 mm and 2 mm) have also been considered thus far. We now illustrate an additional facet of such interactions wherein neither mode is a first harmonic (or, conversely, a subharmonic) of the other. To that end, we consider quadratic interactions between two initially energetic modes with $\lambda_z = 1.5$ mm and $\lambda_z = 2.25$ mm, respectively, and investigate their effect on the evolution of the “difference” mode with a wavelength of 4.5 mm. Figures 9(a) and 9(b) illustrate the variation in chordwise evolution of each of these modes as the initial amplitude of the control input (1.5 mm mode) is increased from a lower initial value (0.0001) to a higher value (0.002). In the course of this variation, only the shorter wavelength modes are seeded at the initial location; the longer 4.5 mm mode is initialized with a relatively small amplitude of 10^{-7} . However, due to a sustained transfer of energy to the longer mode from the shorter wavelength modes, the amplitude of the longer wavelength mode increases with the magnitude of control input. Thus, in Fig. 9(b), the 4.5 mm mode actually becomes the dominant mode at the downstream locations.

The strong intermodal energy transfer noted above is not so surprising, because the linear stationary modes at the respective wavelengths are nearly phase-locked over a significant portion of the chord (consistent with the relatively narrow range of vortex orientations for stationary crossflow modes). For a representative triadic interaction involving stationary modes with wavelengths of 4.5 mm, 2.25 mm and 1.5 mm, respectively, the phase detuning factor (defined as the real part of the complex detuning factor $d_f \equiv [(\alpha_{1.5} - \alpha_{2.25}) - \alpha_{4.5}]/\alpha_{4.5}$) lies within ± 3 percent throughout $x/c > 0.15$ (Fig. 9(c)). Thus, when two modes from a triad have sufficiently large initial amplitudes, nonlinear interactions between the two can easily lead to significant receptivity of the third, unseeded mode. Results from Fig. 9(b) suggest that in some cases, such triadic interactions may favor the excitation of the largest wavelength mode.

Total velocity contours at $x/c \approx 0.41$ pertaining to the triadic interaction are indicated in Fig. 9(d). While analogous to the earlier results for the single mode case in Fig. 6(b), the contours in Fig. 9(d) correspond to relatively smaller disturbance amplitudes. The presence of multiple modes clearly alters the spanwise variation of

the basic state. Depending on the nature of interference between the dominant modes, the multi-mode interactions could result in a smoothing of the spanwise gradients involved (and wall-normal gradients as well, depending on the peak locations for the various modes) for a fixed level of disturbance energy. If this happens, the secondary instability process might be weakened, particularly for the class of modes associated with spanwise gradients of the modified basic state. Observe that the relatively close alignment of vortex axes for various modes (which was responsible for the energy transfer observed in Figs. 9(a)-(b)) is also required to justify a local secondary instability analysis for multi-modal primary disturbances.

We note that, during a separate set of calculations for purely stationary-mode interactions on a low-speed NLF-0415(b) configuration, we had also observed that the effect of interactions between multiple modes of instability are not always intuitive. Specifically, it was found that suppression of the dominant mode may not always be monotonic with respect to the amplitude of the control input, especially when multiple modes and nonparallel mean flows are involved.

2.3 Nonlinear interactions involving traveling mode(s)

The extension of the unit interactions examined in Section 2.2 to more practical cases (including three-mode interactions with dual mode control input and the evolution of a relatively broadband initial spectrum) is currently underway. However, the nonlinear results presented thus far clearly suggest that, even in a higher-Re environment, the growth of the (linearly) most unstable stationary mode can be delayed (even if not suppressed entirely) via nonlinear mode competition with a shorter wavelength mode. However, the effect of non-stationary crossflow modes on this process also needs to be investigated, particularly because of the huge disparity between the linear N factors for the stationary and non-stationary modes. We also note that the ASU experiment was carried out in a conventional supersonic facility, which probably involves a significant level of free-stream unsteadiness due to acoustic radiation from turbulent tunnel-wall boundary layers. However, prior experience with low-speed configurations suggests that the traveling modes are relatively insensitive to acoustic disturbances in the free stream^[54] and their role during the transition process is primarily determined by the level of free-stream vortical fluctuations^[37]. Further work is necessary to clarify the physical mechanisms underlying these observations as well as the relevance of these observations to the supersonic regime.

Saric and Reed^[50] suggest that a byproduct of the artificial roughness would also be to promote a select

subset of the overall spectrum of non-stationary crossflow modes, which is determined by the spatial scales of the roughness. This conjecture seems to be reasonable on physical grounds. It also appears plausible that the physical mechanism underlying roughness-induced excitation of traveling modes is related to the scattering of free-stream unsteadiness (i.e., similar to the roughness-induced excitation of Tollmien-Schlichting and first-mode instabilities studied previously^[22, 45, 15]) rather than attached to any intrinsic unsteadiness in the roughness wakes. However, if the conjectured mechanism is true, then the spatial spectrum of the excited traveling modes may actually be somewhat different from (and perhaps broader than) the roughness spectrum itself, because of the finite spatial scales of free-stream disturbances (especially turbulence, and/or acoustic disturbances in high-speed flows).

Further work is necessary to quantify the details of the abovementioned scattering and its effect on crossflow-induced transition at higher Reynolds numbers. However, it is presently feasible to examine the effect of the stationary control input on the nonlinear evolution of the (linearly more unstable) traveling crossflow modes. This consideration adds to the complexity of the nonlinear interactions examined thus far. This type of calculation for the supersonic, higher-Re configuration considered in this paper has not yet been completed. However, analogous results were obtained earlier for a low-speed NLF-0415(b) configuration (Figs. 10(a)-(b)). That calculation seems to indicate that the same principle which underlies the suppression of the dominant stationary mode may also be applicable to traveling modes (at the same spatial scale as the control input in this particular case). In other words, an additional (desirable) effect of the stationary control input may be reduced amplification of the traveling crossflow modes (relative to their isolated nonlinear development).

The illustrative cases presented in Section 2 indicate potential intricacies of the nonlinear interactions between crossflow instabilities, especially in a high-Reynolds number environment. All of these calculations were based on arbitrarily chosen initial amplitudes of the modes involved. We attempted to vary the initial amplitudes over a logarithmic scale, in order to bracket the range of phenomena encountered in a realistic flow environment. However, given the observed effect of the initial amplitude spectrum on the range of locations where disturbance amplitudes attain significantly large levels (potentially leading to the onset of secondary instabilities), we now investigate the receptivity mechanisms pertaining to the dominant modes involved in those interactions.

3. Receptivity due to small-amplitude surface roughness

Following the theoretical work by Goldstein^[22], Ruban^[45], Fedorov and Khokhlov^[20], Zhong^[58], Wu^[57] and others, plus complementary experiments by Saric et al.^[48] and Maslov et al.,^[34] a large class of important receptivity mechanisms pertaining to both streamwise and crossflow instability modes may be considered to be well-understood at this point. As discussed in ref. [14], surface roughness provides a dominant and preferential source of receptivity for stationary crossflow modes. The receptivity theories of Goldstein and Ruban are easily extended to predict the roughness-induced excitation of stationary crossflow modes in an infinite-span configuration. Specifically, the perturbation q_{ins} associated with an instability mode with a specified wavenumber β along the spanwise (z) direction can be expressed in the form:

$$q_{\text{ins}}(x, y, z; \beta) = A_i(\beta) E(y; x, \beta) \exp[i\theta(x) + i\beta z],$$

where A_i denotes the effective initial amplitude at the location of the source ($x=x_i$); E denotes the shape of this eigenmode along the wall-normal (y) direction at the chordwise location of interest (x); and the complex quantity $\theta(x)$ reflects variations in phase during the propagation of the generated mode from its source location (including any spatial amplification/decay).

In principle, the initial amplitude $A_i(\beta)$ of this mode is given by the convolution between an intrinsic efficiency function for receptivity $\Lambda(x; \beta)$ and the spatial distribution of the surface roughness, with appropriate weighting for the spatial growth or decay of the eigenmode (Eq. (6) from ref. [15]). The efficiency function Λ denotes the part of the Green's function for the overall roughness-induced perturbation that corresponds to the stationary crossflow mode of interest. The convolution integral represents a lumped measure of interference between the instability wave components generated across the chordwise extent of the roughness distribution. For the special case of a localized (yet finite) non-uniformity, the convolution integral reduces to a product between the local value of the efficiency function (i.e., $\Lambda(x_i; \beta)$) and a geometry factor F that corresponds to the Fourier amplitude of the roughness distribution for a chordwise wavenumber that is resonant with the local wavenumber $\alpha \equiv \alpha(\beta)$ of the instability mode. (See ref. [15] for a detailed discussion.)

3.1 Efficiency function for stationary crossflow modes (i.e., influence of roughness location)

Figure 11 indicates the chordwise variation in the magnitude of the efficiency function $\Lambda_u(x; \beta)$ (based on chordwise mean and perturbation velocities and a reference scale given by the similarity scale for boundary-layer flows) for stationary crossflow modes at

selected spanwise wavelengths. An inhomogeneous form of quasi-parallel stability equations (as outlined in Ref. [15]) was used to obtain these predictions. Receptivity is most efficient for roughness array locations close to the attachment line (which is the same as the leading edge because of the symmetric cross section and zero angle of attack); it becomes considerably less effective for roughness locations farther downstream. This trend is generic to stationary crossflow excitation on a variety of swept-wing configurations that have been examined before, both at low speeds^[13, 38, 51] and high speeds^[51].

Coupled with the early onset of linear instability for a broad range of wavelengths over the present configuration, the receptivity predictions in Fig. 11 indicate that the roughness array used as control input towards LFC application would be most effective when placed within first 2-3 percent region of the chord. A second implication is that any natural seeding of other stationary modes via uncontrolled surface roughness also occurs within the leading-edge region. Therefore, it is probably adequate to maintain the surface finish qualities required for LFC applications within a narrow region close to the leading edge; i.e., tolerance levels farther downstream can be allowed to be significantly less restrictive.

3.2 Influence of roughness geometry

As described in ref. [12], the geometry factor for an array of roughness elements with a circular planform is given by

$$F = (2\pi)^{-1/2} \beta/k^2 \Phi \quad (\Phi \equiv kR J_1(kR)).$$

Here, $k = (\alpha^2 + \beta^2)^{1/2} = 2\pi/\lambda_{\text{ins}}$ denotes the effective wavenumber of the instability mode, $\alpha \equiv \alpha(\beta)$ being the chordwise wavenumber for a vortex mode of spanwise wavenumber β ; λ_{ins} is the modal wavelength in the direction orthogonal to the vortex axis; R represents the radius of each roughness element; and J_1 indicates the Bessel function of the first kind and order 1. The factor Φ determines the influence of the roughness size; it is primarily determined by the size of its planform radius compared with the effective instability wavelength λ_{ins} . Fig. 12, reproduced from Ref. [12], indicates the variation in $|\Phi|$ as a function of the non-dimensional element radius R/λ_{ins} , with the scaled growth rate $\text{Im}(k)/\text{Re}(k)$ of the instability mode as a parameter.

For the Reynolds number of interest (16.3 million), the ASU experiments^[50] used an array of roughness dots with a spanwise spacing of 1.7 mm and a nominal diameter of 400 microns. The actual diameter of the dots was, however, estimated to be closer to 500 microns. According to linear stability predictions, $\lambda_{\text{ins}} \approx 0.488$ mm for a stationary crossflow mode with $\lambda_z = 1.71$ mm. Therefore, as indicated by the first peak in Fig. 12, the design diameter of 400 microns is fairly close to the

optimal size of $R/\lambda_{\text{ins}} \approx 0.383$; however, the actual roughness size of 500 micron diameter may have been only marginally less efficient. In a subsequent set of experiments at a lower Reynolds number, Saric and Reed^[50] report using a roughness strip in the form of indentations with a diameter of 200 microns. The smaller roughness elements would have been less effective at $\text{Re}_c = 16.3$ million. However, the magnitude of the geometry factor at the smaller radius also appears to be less sensitive (compared with the 500 micron diameter array) to uncertainties in the roughness size and the predicted instability wavelength. In the present analysis, for example, such uncertainties could result from errors in modeling the geometry and surface pressure distributions from Ref. [50] using a digitizing process.

We find that the initial amplitudes of the 1.5 mm mode based on the receptivity analysis presented above are within the range of control inputs required to produce delayed growth of the dominant mode (as considered during the nonlinear PSE calculations in Section 2). Yet, we caution that the analytical simplification associated with receptivity predictions for a localized array of roughness elements requires the mean-flow variation in x to be sufficiently slow, that both the stability and receptivity characteristics of the boundary-layer flow (contained within the convolution integral mentioned previously) may be adequately approximated by their local behavior. Because of the rapid variation in $\Lambda(x; \beta)$ near the leading-edge region, this approximation may have a marginal validity in the present case. Previous experience indicates that curvature effects may amplify such variations in $|\Lambda|$, further increasing the overall efficiency of roughness-induced receptivity.^[13, 16, 26] Accordingly, following a validation of the receptivity prediction capability built into the LASTRAC code (based on compressible extension to the adjoint PSE approach in Ref. [19]) via higher fidelity approximations based on the harmonic form of linearized Navier-Stokes equations^[52] and/or full DNS^[28] (as illustrated in the context of Fig. 4 in Section 2.1), we plan to extend the zero-order receptivity predictions presented in this section to include the effects of both mean-flow nonparallelism and surface curvature on the roughness-induced receptivity.

4. Measurement of roughness on an LFC surface

Receptivity models such as those presented in Section 3 cannot be used to quantify the natural excitation of instabilities on a realistic LFC configuration until sufficiently detailed characterization of the natural, broadband disturbance environment is made available. The lack of adequate information concerning both free-stream unsteadiness and surface disturbances (e.g.,

surface roughness and/or waviness) represents a major obstacle in physics based predictions of laminar-turbulent transition. As an initial step in developing the necessary characterization for surface roughness over a range of aerodynamic surfaces, detailed surface profile measurements were made on the baseline (i.e., zero-suction) model used during the NASA-Boeing HLFC experiment.^[13, 31, 53] This experiment was carried out during 1995 in the 8ft Transonic Pressure Tunnel at NASA Langley Research Center.

The measurements were made by the Quality Assurance and Inspection Branch at NASA Langley using a Browne and Sharpe Validator Coordinate Measurement Machine. The data were acquired over ten disjoint stripes on the upper surface of the FLOW-9 airfoil model used during the HLFC experiment (Fig. 13(a)). Measurements over each stripe yielded ten spanwise scans of the airfoil surface at a chordwise spacing of 0.02". The spanwise spacing during each scan was 0.01", providing a total of 8001 points over each stripe.

Figure 13(b) displays selected spanwise wavenumber spectra of the roughness distribution as determined from the above measurements. The possibility of spectral contamination due to the limited precision of the measurement process was minimized via sensitivity analysis. The roughness spectrum is relatively flat across the range of stationary crossflow wavelengths relevant to the conditions of the NASA-Boeing experiment. The root mean square height perturbation across this band of wavelengths is of the order of one micron. For reference, crossflow amplitudes based on deterministic receptivity computations for periodic roughness arrays with an effective cross-sectional area of 500 square microns (in the x-y plane) are consistent with the range of amplitudes measured for the dominant crossflow mode ($\lambda_z = 6$ mm) in the zero-suction case^[13]. Figure 14 illustrates one such measurement from the NASA/Boeing experiment, which was acquired at the 19% chord location. The normalized velocity contours indicated in the figure are analogous to those obtained in the low-speed ASU experiments.^[42]

It is possible to extend deterministic receptivity models to stochastic roughness distributions, so as to characterize the receptivity in a statistical sense (see, e.g., ref. [11]). There are obvious deficiencies with using ensemble averaging over a sample space of aerodynamic surfaces. However, in the present application, the ensemble averaging could be replaced by spanwise averaging if (local) homogeneity in that direction can be established, preferably via measurements over an extended spanwise region. The 8" length of each scan during the FLOW-9 measurements is perhaps too small to establish the homogeneity of roughness distribution over the scale of the model. However, if isotropy holds,

then it might be possible to verify the homogeneity properties along the chordwise direction and, by inference, in z as well. Of course, given the wide range of roughness distributions that may be encountered in practice, further work is necessary both to quantify the uncertainty in the specification of the roughness and to propagate that uncertainty to establish the variability in naturally occurring instability wave amplitudes at a suitable initial location. Also desirable are two-dimensional maps of the roughness distribution (rather than a series of independent spanwise scans as in the FLOW-9 measurements) to allow direct estimates of both chordwise and spanwise spectra.

We also note that any significant outliers were removed (as measurement noise) from the data prior to spectral estimation. However, it is conceivable that the dominant source of receptivity corresponds to actual peaks of this type, in which case the spectral analysis may become less relevant. Wavelet techniques might also be worth exploring in this context.

5. Summary and Concluding Remarks

In this paper, we have examined various aspects of crossflow mode evolution in a supersonic, swept-wing configuration that was recently used to demonstrate the feasibility of roughness based, passive LFC in a Mach 2.4 wind-tunnel experiment at Arizona State University. Although this study is not yet complete, we believe that the preliminary investigation reported herein has provided useful insights into the dynamics of crossflow instabilities in the highly unstable boundary-layer flows characteristic of full-scale application on a supersonic aircraft. Continuation of this effort will focus on the effects of broadband disturbance input, including the role of the more unstable non-stationary modes (whether traveling crossflow or secondary instabilities). At that stage, we will aim to match the experimental conditions as closely as possible, in an attempt to simulate the observed delay in transition. Effects of flight-scale Reynolds number will be investigated in the context of another configuration designed for a separate wind tunnel test of roughness based LFC under the joint auspices of DARPA's QSP and NASA's SVT programs.

Noteworthy findings from the present work include: a seemingly rapid rise of stationary crossflow amplitudes (compared with lower-Re configurations) to levels that may well harbinge the onset of secondary instabilities; potential significance of the relative phase between disturbance modes; and quadratic interactions leading to nonlinear receptivity of larger wavelength modes. These findings, albeit interesting, require further scrutiny to establish their validity (using higher fidelity simulations and/or experiments) as well as their generality (via the follow-on parametric study). The present study also

provides partial justification for the lower fidelity design practices used during the successful demonstration of passive SLFC in the ASU wind-tunnel experiment^[50], including the choice of roughness size and location. However, the findings herein also emphasize a strong need to account for the nonlinear crossflow interactions, partly to minimize the risks involved and to optimize the overall performance. Fortunately, the same findings also hint at the possibility of accomplishing this ambitious goal via a simpler, nonlinear amplitude criterion. The parametric study (together with additional experiments) will help establish the validity of this criterion in the applications of interest.

Equally importantly, we have attempted to make the case for a holistic approach to transition prediction, particularly in the context of advanced LFC concepts such as roughness based control. Additional work is currently underway, both in terms of more refined physical modeling for the individual stages in transition and a tighter integration between the respective prediction modules. Some of the intrinsic challenges in the practical implementation of the holistic approach were also discussed, plus potential ways to overcome those challenges (including a hierarchical approach that may be customized for each class of applications).

A high fidelity approach for transition prediction is particularly difficult to incorporate into design oriented CFD, especially in the context of multi-disciplinary optimization. However, recent work^[30] has shown that individual ingredients of such physics based prediction capability may well provide the foundation for a more efficient approach that is more amenable to inclusion into the MDO process. This will allow a designer to account for the $O(1)$ influence of transition on the performance of an efficient and quiet supersonic aircraft at an earlier stage of the vehicle design process.

Before closing, we emphasize the further need for accurate transition prediction for fully three-dimensional mean flows. Spanwise variations in mean flow add an extra dimension to the complexity of transition prediction, also increasing the uncertainties in the predictions made. Our future work will focus on extending the holistic/hierarchical prediction methodology to flows of this type.

Acknowledgments

The authors gratefully acknowledge the contributions of Dr. Li Jiang from the University of Texas at Arlington during the validation of the LASTRAC code. We would also like to thank Brian Howerton of Lockheed Martin for documenting the roughness measurements outlined in Section 4.

References

1. Anders, S.G. and Fischer, M.C., "F-16XL-2 Supersonic Laminar Flow Control Flight Test Experiment," NASA TP-1999-209683, 1999.
2. Bertolotti, F.P., Herbert, Th., and Spalart P., "Linear and Nonlinear Stability of the Blasius Boundary Layer," J. Fluid. Mech., vol. 242, pp. 441-474, 1992.
3. Bushnell, D., Proc. "Applications and Suggested Directions of Transition Research," Fourth Symp. on Numerical And Physical Aspects of Aerodynamic Flows," Long Beach, CA, Jan. 16-19, 1989.
4. Cattafesta, III L.N., Iyer, V., Masad, J.A., King, R.A., and Dagenhart, J.R., "Three-Dimensional Boundary-Layer Transition on a Swept Wing at Mach 3.5," AIAA J., vol. 33, No. 11, pp. 2032-37, 1995.
5. Chang, C.-L., "ECLIPSE: An Efficient Compressible Linear PSE Code for Swept-Wing Boundary Layers," High Technology Report No. HTC-9503, 1995.
6. Chang, C.-L., Vinh, H., and Malik, M.R., "Hypersonic Boundary-Layer Stability with Chemically Reactions Using PSE," AIAA Paper97-2012, 1997.
7. Chang, C.-L., "Thermal Effect on Crossflow Instability in Supersonic Boundary Layers," Proc. 14th US National Congress of Theoretical and Applied Mechanics, Roanoke, VA, June 2002.
8. Chang, C.-L., "The Langley Stability and Transition Analysis Codes (LASTRAC: LST, Linear and Nonlinear PSE for 2D, Axisymmetric, and Infinite Swept Wing Boundary Layers," AIAA Paper 2003-0974, 2003.
9. Chang, C.-L., Malik, M.R., Erlebacher, G., and Hussaini, M.Y., "Compressible Stability of Glowing Boundary Layers Using Parabolized Stability Equations," AIAA Paper 91-1636, 1991.
10. Chang, C.-L., Malik, M.R., and Vinh, H., "Linear and Nonlinear Stability of Compressible Swept-Wing Boundary Layers," AIAA Paper 95-2278, 1995.
11. Choudhari, M., "Boundary-Layer Receptivity due to Distributed Surface Imperfections of a Deterministic or Random Nature," Theor. Comput. Fluid Dynamics, Vol. 4, No. 3, pp. 101-117, 1993.
12. Choudhari, M., "Roughness-Induced Generation of Crossflow Vortices in Three-Dimensional Boundary Layers," Theor. Comp. Fluid Dyn., vol. 5, pp. 1-31, 1994.
13. Choudhari, M.M., Li, F., Chang, C.-L., and Malik, M.R., "NASA/Boeing HLFC Experiment: Data Analysis with Advanced CFD Tools," HTC Report-9607, June 1996.

14. Choudhari, M. and Streett, C.L., "Boundary Layer Receptivity Phenomena in Three-Dimensional and High-Speed Boundary Layers," AIAA Paper 90-5258, 1990.
15. Choudhari, M. and Streett, C.L., "Theoretical Prediction of Boundary-Layer Receptivity," AIAA Paper 94-2223, 1994.
16. Collis, S. and Lele, S., *J. Fluid Mech.*, "Receptivity to Surface Roughness near a Swept Leading Edge," vol. 380, pp. 141-168, 1999.
17. Crouch, J.D., "Receptivity of Boundary Layers," AIAA Paper 94-2224, 1994.
18. Crouch, J.D., "Transition Prediction and Control for Airplane Applications," AIAA Paper 97-1907, 1997.
19. Dobrinsky, A. and Collis, S.S., "Adjoint Parabolized Stability Equations for Receptivity Prediction," AIAA Paper 2000-2651, 2000.
20. Fedorov, A.V., and Khokhlov, A. P., "Excitation of Unstable Modes in a Supersonic Boundary Layer by Acoustic Waves," *Izv. Akad. Nauk SSSR, Mekh. Zhidk. Gaza*, No. 4, pp. 67-74, 1991.
21. Fedorov, A.V., Malmuth, N.D., Rasheed, A., and Hornung, H., "Stabilization of hypersonic boundary layers by porous coatings," AIAA Paper 2001-0891, 2001.
22. Goldstein, M.E., "Scattering of Acoustic Waves into Tollmien-Schlichting Waves by Small Streamwise Variations in Surface Geometry," *J. Fluid Mech.*, Vol. 154, pp., 509-529, 1985.
23. Haynes, T., and Reed, H.L., "Computations in Nonlinear Saturation of Stationary Crossflow Vortices in a Swept-Wing Boundary Layer," AIAA Paper 96-0182, 1996.
24. Herbert, Th., "Parabolized Stability Equations," *Ann. Rev. Fluid Mech.*, vol. 20, pp. 245-283, 1997.
25. <http://www.aerospace.nasa.gov/goals/fsvtp.html> (Also: Coen. P.G., private communication, 2002.)
26. Janke, E., "Receptivity and Transition Control of Swept-Wing Boundary-Layers; Effects of Surface Curvature and Nonlinearity," AIAA Paper 2001-2980, 2001.
27. Janke, E. and Balakumar, P., "Transition Control Using Leading Edge Roughness," AIAA Paper 99-3656, 1999.
28. Jiang, L., Chang, C.-L., Choudhari, M., and Liu, C., "Cross-Validation of DNS and PSE Results for Instability-Wave Propagation in Compressible Boundary Layers," Submitted to 16th AIAA Computational Fluid Dynamics Conference, Orlando, Florida, June 23-26, 2003.
29. Jiang, L., Shan, H., Liu, C., & Visbal, M., "Non-reflecting boundary conditions in curvilinear coordinates," 2nd AFOSR International Conference on DNS/LES, June, 1999, Edited by D. Knight and L. Sakell.
30. Kroo, I., Sturza, P., Tracey, R., and Chase, J., "Natural Laminar Flow for Quiet and Efficient Supersonic Aircraft," AIAA Paper 2002-0146, 2002.
31. Li, F., Choudhari, M.M., Wie, Y-S, Radeztsky, R., Chang, C.-L., and Malik, M.R., "NASA/Boeing HLFC Experiment: Data Analysis," High Technology Report HTC-9610, Oct. 1996.
32. Malik, M.R., "Boundary-Layer Transition Prediction Toolkit," AIAA Paper 97-1904, 1997.
33. Malik, M.R., Li, F., Choudhari, M., and Chang, C.-L., "Secondary Instability of Crossflow Vortices and Swept-Wing Boundary Layer Transition," *J. Fluid Mech.*, vol. 399, pp. 85-115, 1999.
34. Maslov, A.A., Shplyuk, A. N. , Sidorenko, A. A. , and Arnal, D., "Leading-Edge Receptivity of a Hypersonic Boundary Layer on a Flat Plate," *J. Fluid Mech.*, Vol. 426, pp. 73-94, 2001.
35. Maslov, A.A., Mironov, S. G. , Buntin, D. A. , Sidorenko, A. A. , Shplyuk, A. N. , and Aniskin, V. M., "Hypersonic flow stability experiments," AIAA Paper 2002-0153, 2002.
36. Monkewitz, P.A., "Subharmonic Resonance, Pairing, and Shredding in the Mixing Layer," *J. Fluid Mech.*, Vol. 188, pp. 223-252, 1988.
37. Muller, B. and Bippes, H., "Experimental Study of Instability Modes in a Three-Dimensional Boundary Layer," In *Fluid Dynamics of Three-Dimensional Turbulent Shear Flows and Transition*, AGARD CP-438, 1989.
38. Ng, L., and Crouch, J.D., "Roughness-Induced Receptivity to Crossflow Vortices on a Swept Wing," *Phys. Fluids*, vol. 11, No. 2, pp. 432-438, 1999.
39. NRC Committee on Breakthrough Technology for Commercial Supersonic Aircraft, "Commercial Supersonic Technology – The Road Ahead," Aeronautics and Space Engineering Board, National Research Council, 2002.
40. Pruett, C. D., Chang, C.-L., and Streett, C.L., "Simulation of Crossflow Instability on a Supersonic Highly Swept Wing," *Comp. And Fluids*, vol. 29, pp. 33-62, 2000.
41. Reed, H.L., Haynes, T.S. and Saric, W.S., "Computational Fluid Dynamics Validation Issues in Transition Modeling," *AIAA J.*, Vol. 36, No. 5, pp, 742-751, May 1998.
42. Reibert, M.S. and Saric, W.S., "Review of Swept-Wing Transition," AIAA Paper 97-1816, 1997.
43. Reshotko, E., "Boundary-Layer Stability and Transition," *Ann. Rev. Fluid Mech.*, Vol. 8, pp. 311-349, 1976.
44. Reshotko, E., "Boundary-Layer Instability, Transition and Control," AIAA Paper 94-0001, 1994.
45. Ruban, A.I., "On the Generation of Tollmien-Schlichting Waves by Sound," *Fluid Dyn.*, Vol. 19, pp. 709-16, 1985.

46. Rubinstein, R., and Choudhari, M., "A Statistical Theory of Transition," ICASE Report 2000-50, 2000.
47. Saric, W.S., Carrillo, Jr. R.B., and Reibert, M., "Leading-Edge Roughness as a Transition Control Mechanism," AIAA Paper 98-0781, 1998.
48. Saric, W.S., Hoos, J.A., and Radeztsky, R.H., "Boundary Layer Receptivity of Sound with Roughness," In Boundary-Layer Stability and Transition to Turbulence, ed. D.C. Reda, H.L. Reed, and R. Kobayashi (ASME, New York), FED Vol. 114, pp. 77-82, 1991.
49. Saric, W.S., Kozlov, V.V., and Levchenko, V. Ya., "Forced and Unforced Subharmonic Resonance in Boundary-Layer Transition," AIAA Paper 84-0007, 1984.
50. Saric, W.S. and Reed, H.L., "Supersonic Laminar Flow Control on Swept Wings Using Distributed Roughness," AIAA Paper 2002-0147, 2002.
51. Singer, B.A. and Choudhari, M., "Receptivity Prediction for Swept-Wing Boundary Layers," NASA Research Highlight, 1995.
52. Streett, C.L., "Direct Harmonic Linear Navier-Stokes Methods for Efficient Simulation of Wave Packets," AIAA Paper 98-0784, 1998.
53. Streett, C.L., "Designing a Hybrid Laminar-Flow Control Experiment via CFD," AIAA Paper 2003-0977, 2003.
54. Waitz, I.A. and Wilkinson, S.P., "Rotating Disk Transition due to Isolated Roughness with Intense Acoustic Radiation," AIAA Paper 88-3759, 1988.
55. Wie, Y.-S., "BLSTA – A Boundary Layer Code for Stability Analysis," NASA CR 4481, 1992.
56. Wlezien, R.W. and Veitch, L., "Quiet Supersonic Platform Program Advanced algorithms for design and optimization of Quiet Supersonic Platforms," AIAA Paper 2002-0143, 2002.
57. Wu, X., "Generation of Tollmien-Schlichting Waves by Convecting Gusts Interacting with Sound," J. Fluid Mech., Vol. 397, pp. 285-316, 1999.
58. Zhong, X., "Direct Numerical Simulation of Hypersonic Boundary-Layer Transition over Blunt Leading Edges, Part II: Receptivity to Sound," AIAA Paper 97-0756, 1997.

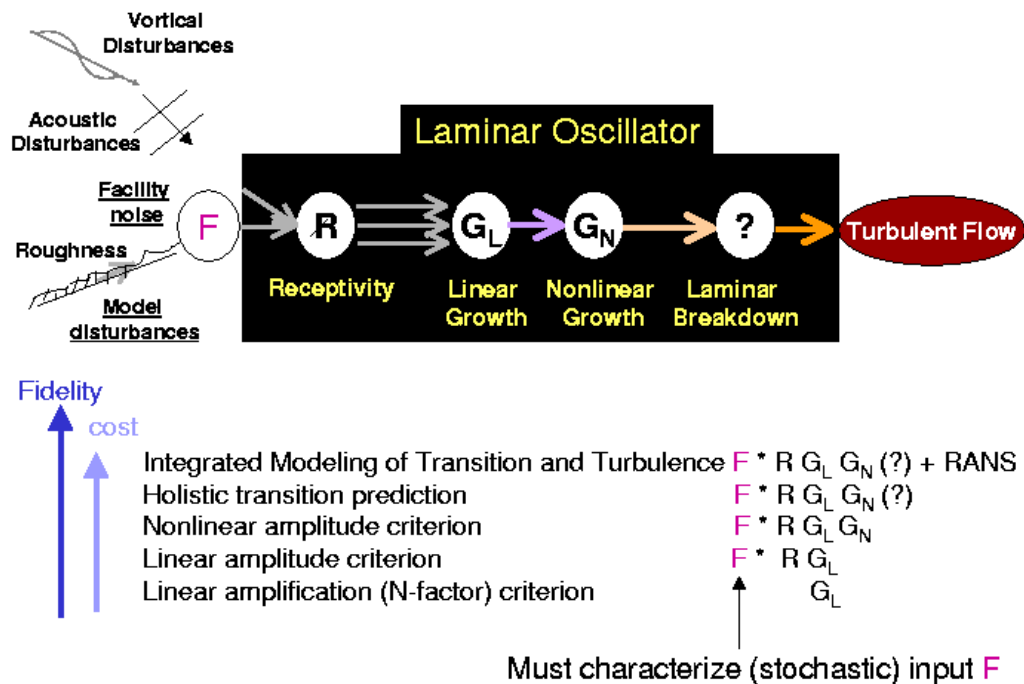
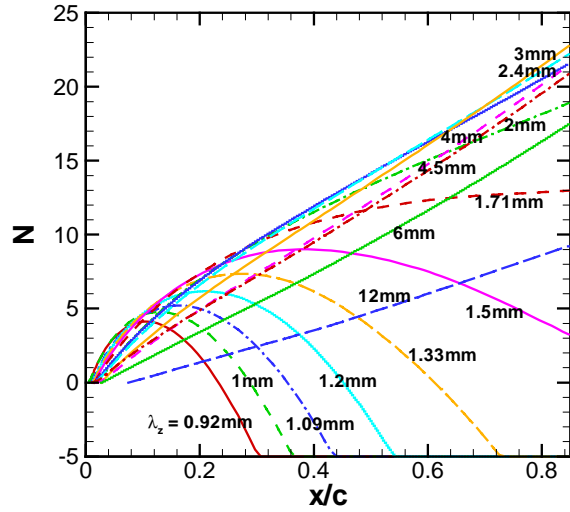
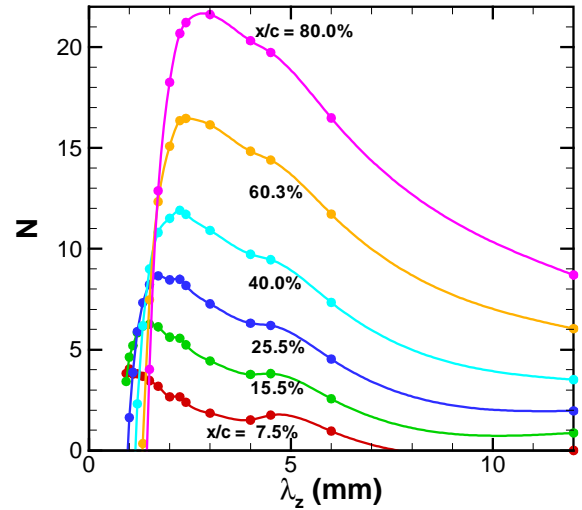


Figure 1. Schematic of hierarchical levels of transition prediction from a systems viewpoint. The holistic prediction approach, based on transition as a forced response of a nonlinear system to stochastic forcing,^[43] appears near the top of this hierarchy. The parenthesized question mark denotes the state of affairs in regard to bridging the gap between physics based modeling preceding the laminar breakdown phase and some form of statistical turbulence modeling farther downstream.^[46]



2(a) N-factor variation along the chord for selected disturbance wavelengths



2(b) N-factor variation at select chordwise locations as function of disturbance wavelength

Figure 2. N-factor predictions for stationary crossflow modes in an infinite-span swept-wing boundary layer modeling the Mach 2.4 ASU wind tunnel configuration at $Re_c = 16.3$ million (linear PSE results including the effects of surface curvature)

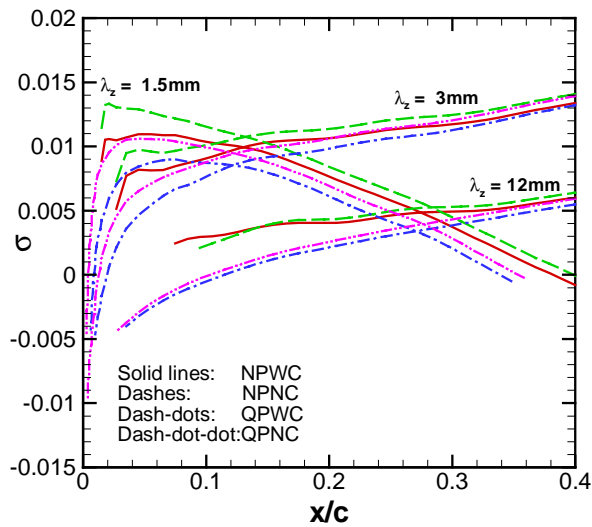


Figure 3. Effects of nonparallelism and surface curvature on growth rates of stationary crossflow vortices (solid lines: linear PSE with curvature (NPWC); dashed lines: linear PSE, no curvature (NPNC); dash dot: quasi-parallel with curvature (QPWC); dash-dot-dot: quasi-parallel, no curvature (QPNC))

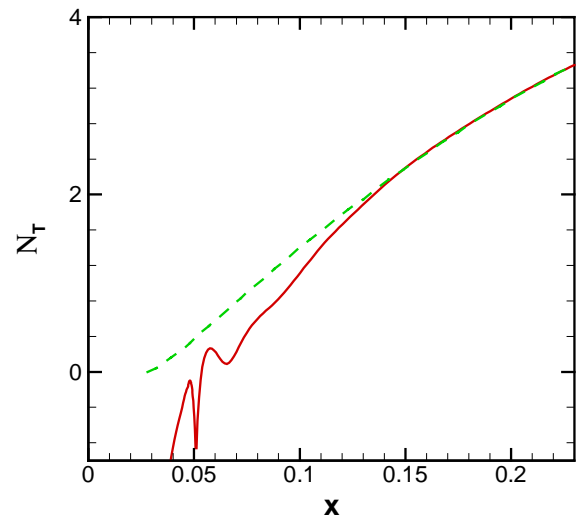
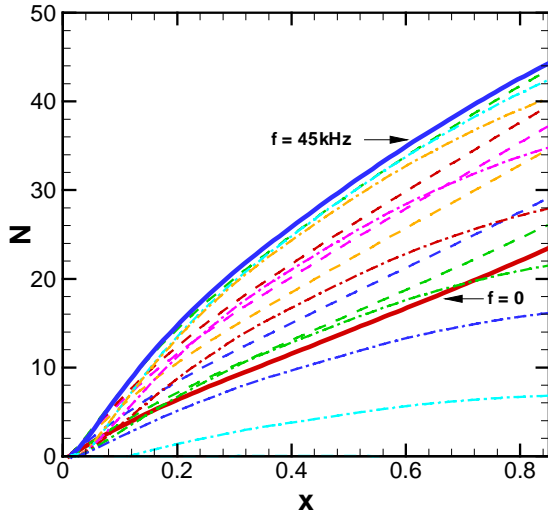
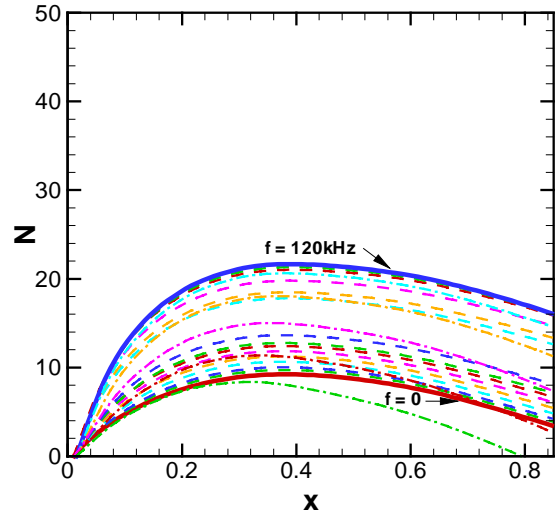


Figure 4. Comparison between stationary N factors based on LASTRAC predictions (dashed line) and a DNS computation (solid line) based on the DNSUTA code by Jiang, Shan and Liu from the University of Texas at Arlington.^[29] The vertical axis denotes nonparallel N-factor based on peak temperature perturbation.

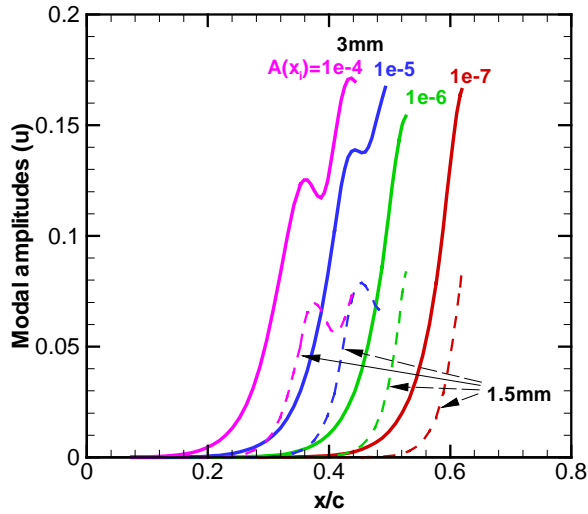


5(a) $\lambda_z = 3\text{mm}$ (Dashed lines: $0 < f < 45\text{kHz}$; dash-dots: $45\text{kHz} < f < 85\text{kHz}$)



5(b) $\lambda_z = 1.5\text{mm}$ (Dashed lines: $0 < f < 120\text{kHz}$; dash-dots: $f > 120\text{kHz}$)

Figure 5. N-factors for traveling crossflow modes



6(a) Nonlinear evolution of most unstable stationary crossflow mode ($\lambda_z = 3\text{mm}$) for varying initial amplitudes $A(x_i)$. Chordwise variation of modal amplitudes is indicated for the fundamental mode and its first harmonic ($\lambda_z = 1.5\text{mm}$)

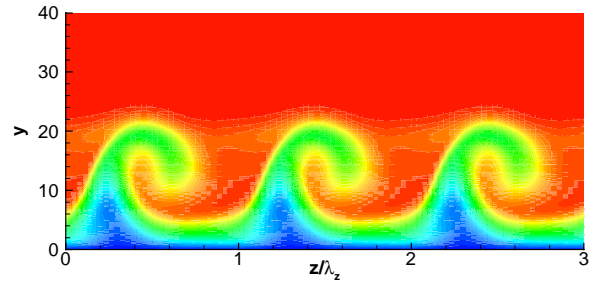
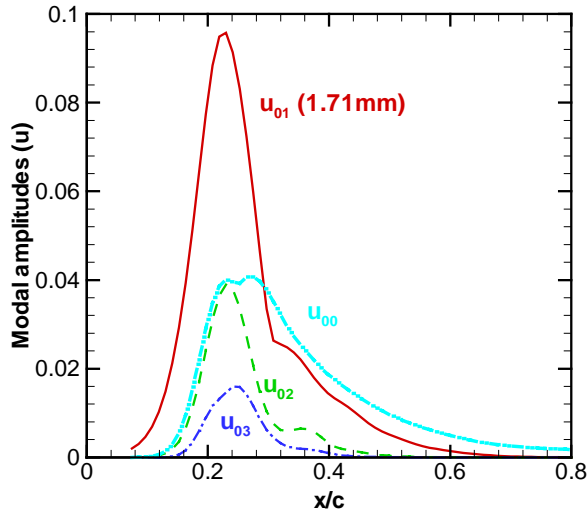
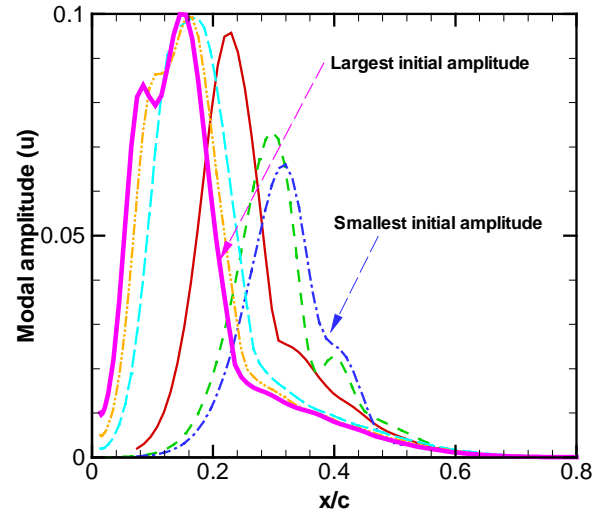


Figure 6(b) Contours of normalized total velocity component along the local inviscid streamline in a plane transverse to the vortex axis. Disturbance parameters correspond to the case $A(x_i) = 10^{-7}$ in Fig 6(a); the chordwise location for the contours corresponds to $x/c \approx 0.62$.

Figure 6(a)-(b). Nonlinear evolution of most unstable stationary crossflow mode

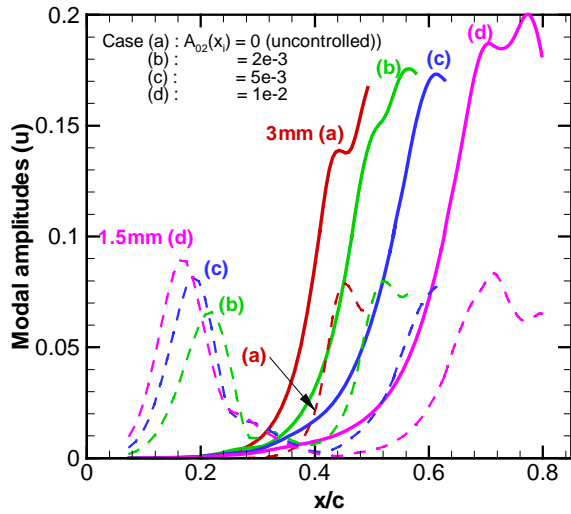


6(c): Evolution of various harmonics for a fixed initial amplitude of the $\lambda_z = 1.71$ mm mode ($A(x_i) = 0.002$)

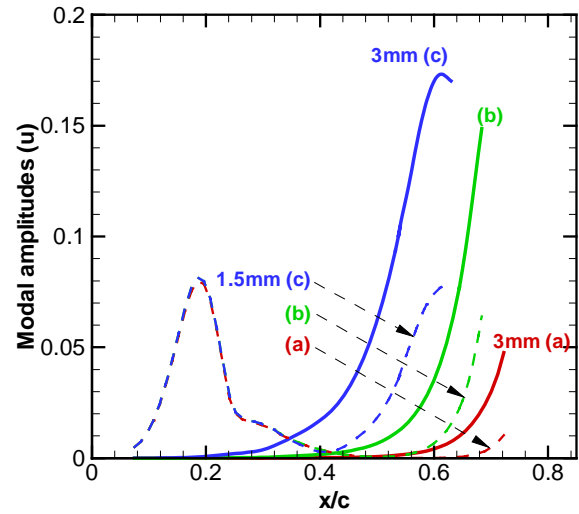


6(d): Fundamental evolution as function of the initial amplitude of $\lambda_z = 1.71$ mm mode.

Figure 6(c)-(d) Nonlinear evolution of a subdominant stationary mode suitable for control input towards roughness based LFC



7(a): Nonlinear control of most unstable mode ($\lambda_z = 3$ mm) via control input with different initial amplitudes of $\lambda_z = 1.5$ mm mode.



7(b). Effect of initial amplitude of the target mode ($\lambda_z = 3$ mm) for a fixed amplitude of control input ($A_{1.5 \text{ mm}}(x_i) = 0.005$). Cases (a), (b), and (c) correspond to $A_{3 \text{ mm}}(x_i) = 1e-7, 1e-6$ and $1e-5$, respectively.

Figure 7. Assessment of roughness based LFC on the Mach 2.4 ASU configuration in an elementary context

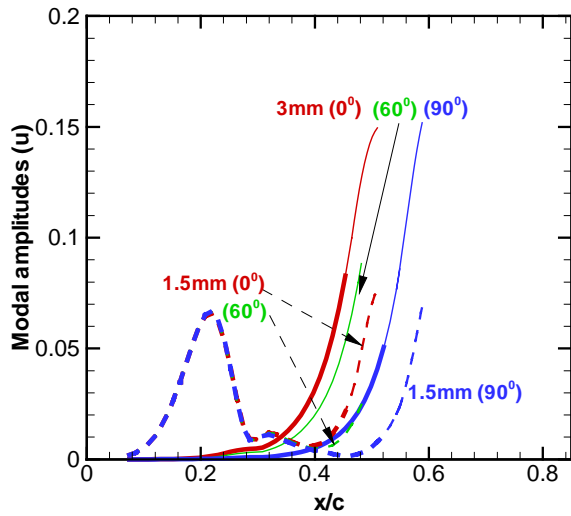


Figure 8. Nonlinear control of most unstable mode ($\lambda_z = 3$ mm) via control input at $\lambda_z = 1.5$ mm: effect of relative initial phase between control input and target mode. Thicker portions of the curves at 0° and 90° denote results obtained with a higher convergence tolerance during nonlinear iterations.

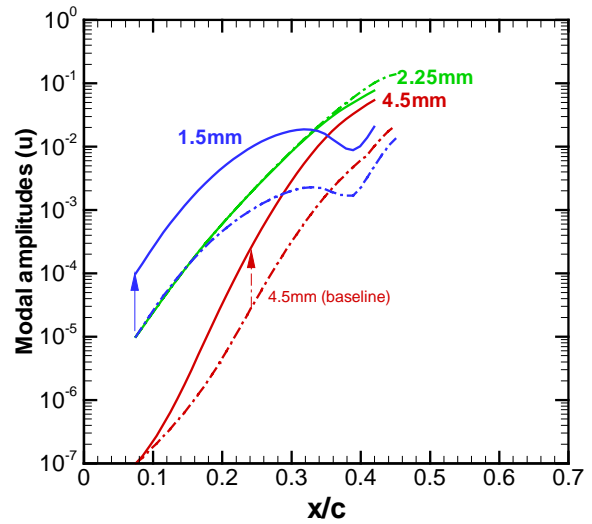
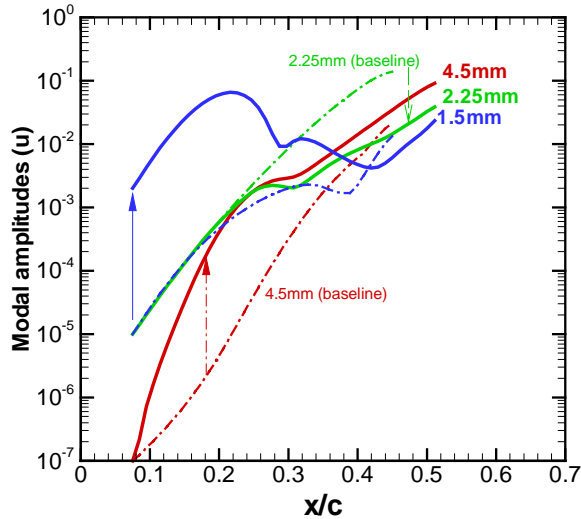
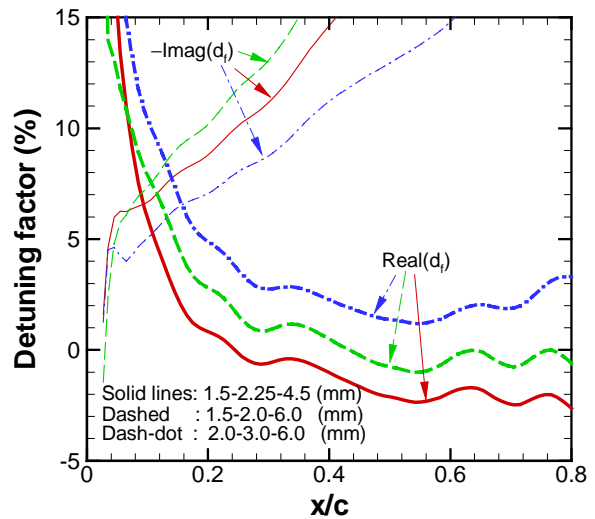


Figure 9(a) Smaller control input ($A_{1.5 \text{ mm}}(x_i) = 0.0001$)
The baseline case corresponds to zero control input; arrows indicate shifts in modal evolution relative to baseline case.



9(b) Larger control input ($A_{1.5 \text{ mm}}(x_i) = 0.002$)



9(c) Detuning factor for triadic interactions between stationary crossflow modes

Figure 9: Nonlinear Receptivity of longer wavelength mode ($\lambda_z = 4.5$ mm) via difference interaction between a pair of shorter wavelength modes ($\lambda_z = 1.5$ mm and $\lambda_z = 2.25$ mm).

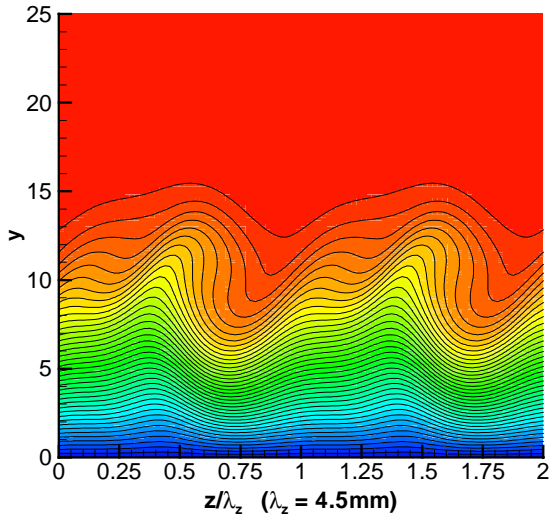
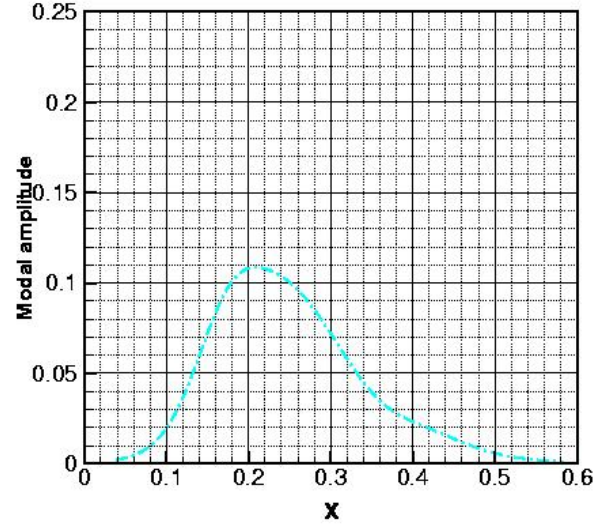


Figure 9(d): Contours of total velocity component along the local direction of the inviscid streamline in a plane transverse to the vortex axis. Flow conditions correspond to those in Fig. 9(b), where the 4.5 mm mode becomes dominant ($x/c \approx 0.41$)



10(a) Traveling mode only
Figure 10. Suppression of traveling crossflow mode via stationary control input.

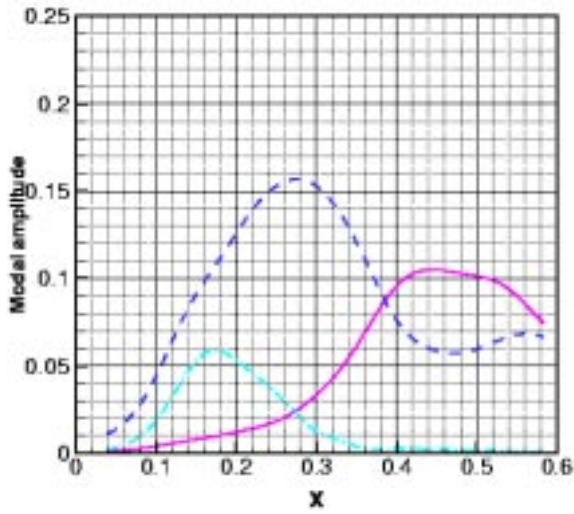


Figure 10(b) Traveling mode with the same initial amplitude, plus two stationary modes involved in roughness-based LFC. (solid line: target stationary mode dashes: stationary control input dash-dot: traveling mode)

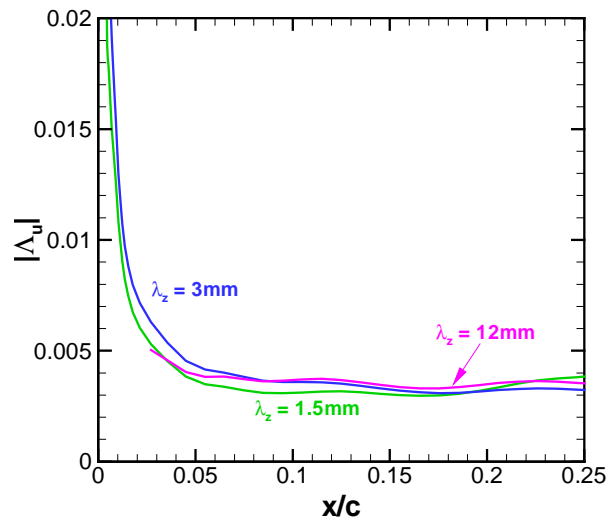


Figure 11: Efficiency function magnitude for roughness-induced excitation of stationary crossflow modes on Mach 2.4 ASU configuration

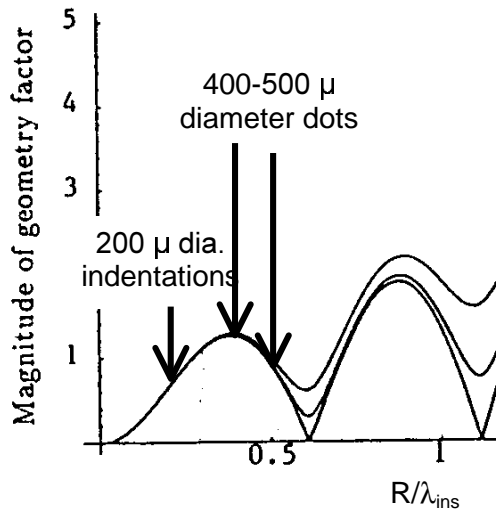
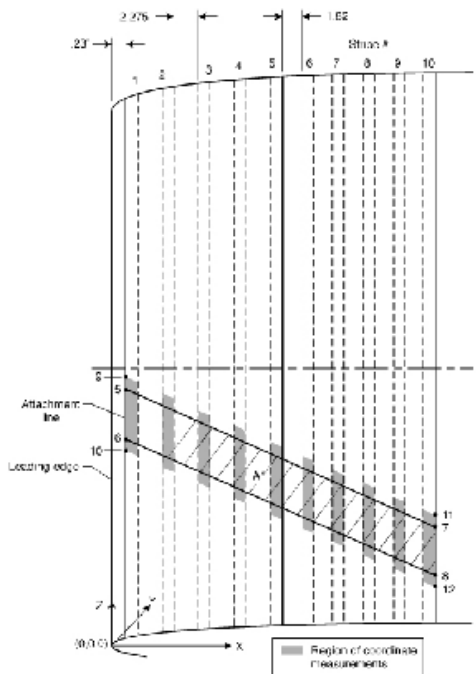
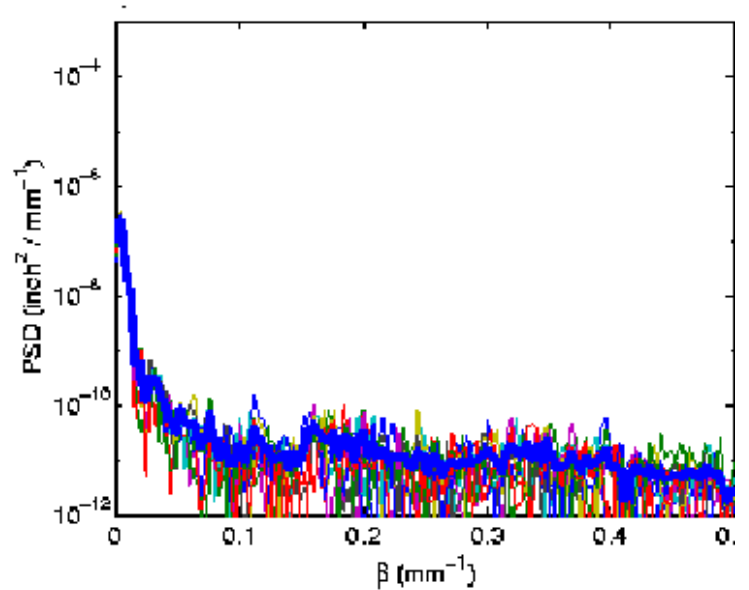


Figure 12: Effect of planform radius of cylindrical roughness elements on receptivity (based on Fig. 6 in ref. [12]). The bottom curve corresponds to locally neutral vortex ($\text{Im}(k)=0$); the other two curves correspond to $\text{Im}(k)/\text{Re}(k) = 0.05$ and 0.1 , respectively.



13(a) Schematic of roughness measurement region (indicated via gray stripes).



13(b) Roughness spectrum inferred from profilometer measurements

Figure 13: Roughness measurements on zero-suction panel of FLOW-9 wing used in NASA/Boeing HLFC experiment

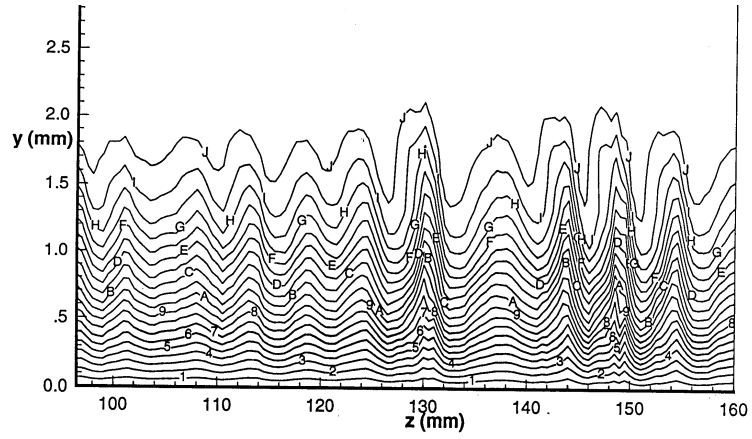


Figure 14: Normalized mean velocity (U/U_0) contours based on hot-wire measurements during NASA/Boeing HLFC experiment (chordwise location: $x/c=0.19$)^[13]